Carbohydrate Polymers 92 (2013) 2128–2134

Contents lists available at SciVerse ScienceDirect

Carbohydrate Polymers

journal homepage: www.elsevier.com/locate/carbpol

Tunable green oxygen barrier through layer-by-layer self-assembly of chitosan and cellulose nanocrystals

Fei Li[a], Paolo Biagioni[b], Marco Finazzi[b], Silvia Tavazzi[c], Luciano Piergiovanni[a,*]

[a] DeFENS – Department of Food, Environmental and Nutritional Sciences, Packaging Division, Università degli Studi di Milano, Via Celoria, 2, 20133 Milano, Italy
[b] Dipartimento di Fisica and CNISM, Politecnico di Milano, Piazza L. da Vinci, 32, 20133 Milano, Italy
[c] Dipartimento di Scienza dei Materiali, Università degli Studi di Milano Bicocca, Via Cozzi, 53, I-20125 Milano, Italy

ARTICLE INFO

Article history:
Received 12 September 2012
Received in revised form
16 November 2012
Accepted 17 November 2012
Available online 7 December 2012

Keywords:
Oxygen barrier
Flexible packaging
Layer-by-layer coating
Cellulose nanocrystals
Chitosan
Packaging sustainability

ABSTRACT

We address the oxygen-barrier properties of a nanocomposite created by layer-by-layer assembly of two biopolymers, chitosan (CS) and cellulose, in nanocrystals form (CNs), on an amorphous PET substrate. We systematically investigated the oxygen permeability, morphology, and thickness of the nanocomposite grown under two different pH combinations and with different number of deposition cycles, up to 30 bilayers. Noticeably, the thickness of each deposited bilayer can be largely tuned by the pH value of the solution, from ~7 up to ~26 nm in the tested conditions. By our analysis, it is reliably concluded that such CS/CNs nanocomposite holds promises for gas barrier applications in food and drug packaging as a clear coating on plastic films and tridimensional objects, improving performance and sustainability of the final packages.

1. Introduction

High gas-barrier materials are crucial components in critical applications, such as food and drug packaging (Cooper, Douglas, & Perchonok, 2011; Priolo, Gamboa, Holder, & Grunlan, 2010; Svagan et al., 2012). In particular, due to their oxygen permeability, conventional plastic films are very often not suitable to assure the long shelf lives required for a wide variety of foods and expected by the market (Cooper et al., 2011). The solution of such a tough problem, in any case, cannot neglect environmental issues: films should efficiently prevent oxygen from penetrating to food, whilst it is recommended that the barrier materials or coatings should be sustainable and environmentally friendly (Svagan et al., 2012).

So far, the main strategies to increase the barrier properties of flexible and transparent materials for food packaging applications have been limited to vacuum metallization, silicon oxide (SiO_x) coatings (Jang, Rawson, & Grunlan, 2008; Leterrier, 2003), manufacturing of multi-layers (by co-extrusion and/or laminating) (Affinito et al., 1996), or development of clay-nanocomposites (Chang, An, & Sur, 2003; Donadi, Modesti, Lorenzetti, & Besco, 2011; Ghasemi, Carreau, Kamal, & Tabatabaei, 2012). However, these solutions do not completely fulfill the sustainability expectations and the needs of transparency, while some technological drawbacks still exist. For instance, SiO_x vapor-deposited thin films are prone to cracking when flexed and show poor adhesion to plastic substrates (Leterrier, 2003); multilayer materials can also present adhesion problems denoting delaminating occurrences; nanoclay-reinforced polymer composites and metallized films suffer from low transparency and relatively high values of the oxygen transmission rate (Osman, Rupp, & Suter, 2005; Sánchez-Valdes, López-Quintanilla, Ramírez-Vargas, Medellín-Rodríguez, & Gutierrez-Rodriguez, 2006). Also, although the most claimed option to increase gas barrier properties of flexible packaging materials is currently represented by nanoclays inclusions (Jang et al., 2008; Priolo et al., 2010; Svagan et al., 2012), yet it was demonstrated that various nanoclays are highly cytotoxic, posing a possible risk to human health (Lordan, Kennedy, & Higginbotham, 2011). Ideally, a barrier coating made of natural bio-polymers could achieve all the goals of high transparency, low gas permeability, bio-compatibility, sustainability and good adhesion. Layer-by-layer (LbL) assembly is a basic technique for the fabrication of multicomponent films on solid supports by controlled adsorption from solutions or dispersions (Decher, 1997) and is also considered as a potential means for implementing new and versatile surface applications including gas barrier coatings (Jang et al., 2008; Priolo et al., 2010; Svagan et al., 2012; Yang, Haile, Park, Malek, & Grunlan, 2011), anti-fog and super-hydrophobic

* Corresponding author at: Via Celoria, 2 20133 Milan, Italy.
Tel.: +39 02 50316638; fax: +39 02 50316672.
E-mail address: Luciano.Piergiovanni@unimi.it (L. Piergiovanni).

0144-8617/$ – see front matter © 2012 Elsevier Ltd. All rights reserved.
http://dx.doi.org/10.1016/j.carbpol.2012.11.091

coatings (Nuraje, Asmatulu, Cohen, & Rubner, 2010; Zhai, Cebeci, Cohen, & Rubner, 2004; Zhang & Sun, 2010), antimicrobial surfaces (Dvoracek, Sukhonosova, Benedik, & Grunlan, 2009; Etienne et al., 2005), drug delivery (Chung & Rubner, 2002; Kim, Park, & Hammond, 2008), and electrically conductive films (Daiko, Katagiri, & Matsuda, 2008; Park, Ham, & Grunlan, 2010). When a nanofiller needs to be integrated within a polymer matrix in order to provide it with specific novel functionalities, LbL techniques represent a means to avoid aggregation and thus achieve a high level of dispersion and a large filler load.

Since cellulose nanocrystals and chitosan come from the first and second most abundant natural polymers on the earth (de Mesquita, Donnici, & Pereira, 2010), their sustainability seems beyond doubt. Due to its nontoxicity, biodegradability, and antimicrobial properties, chitosan has been widely applied to food packaging and medical fields as a polycationic material (Muzzarelli, 2009; Muzzarelli et al., 2012; Ravi Kumar, 2000), whilst cellulose nanocrystals recently gained a great attention as optically transparent reinforcement and barrier coatings (Eichhorn et al., 2010; Kontturi et al., 2007; Sanchez-Garcia, Lopez-Rubio, & Lagaron, 2010) and were found to have neither genotoxicity nor effects on survival and growth of nine aquatic species in the ecotoxicological tests conducted so far (Kovacs et al., 2010). Furthermore, cellulose nanofibers were reported as effective gas barriers, also thanks to their high degree of crystallinity and strong hydrogen bonds: casted coatings based on TEMPO-oxidized cellulose nanofibers (TOCNs) reduced the oxygen permeability (PO_2) of bare poly lactic acid (PLA) and PET films (Fukuzumi, Saito, Iwata, Kumamoto, & Isogai, 2008; Kato, Kaminaga, Matsuo, & Isogai, 2005). Recently, well-controlled LbL assembly of CNs/CS multilayers has been proposed as a novel solution to improve the performance of chitosan coatings by exploiting the large electrostatic interaction and hydrogen bonds with CNs nanofillers (de Mesquita et al., 2010; Qi, Saito, Fan, & Isogai, 2012). At present, however, the barrier properties of such nanocomposites, as well as the influence of pH values on the assembly process, have not yet been fully investigated.

The aim of our work refers to the development of a bionanocomposite coating, able to enhance the gas barrier properties of one of the currently most used synthetic plastics, maintaining its intrinsic transparency and reducing the environmental impact of the coated materials, lowering their final thickness. Our goal was also the full comprehension of the mechanism involved in the nanocomposite growth, in order to be able to modulate the final thickness and porosity, leading to a possible design of the barrier properties.

2. Experimental

2.1. Materials

Shellfish chitosan (CS, GiustoFaravelli SpA, Milan, Italy) had a degree of deacetylation of 85% and a molecular weight ranging from 50,000 to 60,000 (data provided by the supplier). Cotton linter board, provided by SSCCP (Italian pulp and paper research institute, Milan, Italy), was used for producing cellulose nanocrystals. Amorphous poly(ethylene terephthalate) (A-PET, ~180 μm thick) was used as the plastic substrate for layer-by-layer coating, provided from ILPA srl (Bazzano, Italy). Other reagents were purchased from Sigma–Aldrich, Italy.

2.2. Preparation of biopolymer dispersions for layer-by-layer coating

1 wt% chitosan water dispersion was prepared by dissolving the polysaccharide in 0.1 M HCl(aq) at 25 °C for 3 h under stirring. After adjusting pH and filtration, the chitosan dispersion was used for the layer-by-layer coating.

1 wt% cellulose nanocrystals (CNs) water dispersion was prepared from cotton linter using a procedure already established for cotton from powdered filter paper (Dong, Kimura, Revol, & Gray, 1996). Briefly, milled cotton linter was hydrolyzed by 64% (wt/wt) sulfuric acid with vigorous stirring at 45 °C for 45 min. The reaction mixture was diluted with 10 times-volume deionized water (18.2 MΩ cm, Millipore Milli-Q Purification System) and settled for 2 h, and then was rinsed and centrifuged at 5000 rpm repeatedly until the supernatant became turbid. Further purification was then done by dialysis against deionized water until the effluent remained at neutral pH (Molecular Weight Cut Off 12,000 and higher). Sequentially, the suspension was sonicated (UP400S 400 W, Hielscher Co., Germany) repeatedly (5 cycles of 10 min at 70% output) to create cellulose crystals of colloidal dimensions. Finally, the suspension was filtered under vacuum with Muktell (grade GF/C, 1.2 μm) and Whatman glass microfiber filter (grade GF/F, 0.7 μm) to remove contamination and big aggregations. The CNs content of the resulting aqueous suspension was determined by drying several samples (1 ml) at 105 °C for 15 min intervals (to avoid decomposition or burning) until weight constancy, giving a cellulose concentration of ~1% wt/wt and a yield of ~50%.

2.3. Surface charge density measurements

Surface charge densities were measured by means of conductometric titration. For the CNs dispersion, a commercial particle charge detector was used (PCD-04, Müteck, Germany), while for the chitosan dispersion, the same procedure described by Farris, Mora, Capretti, and Piergiovanni (2012) was employed.

2.4. Layer-by-layer assembly

Glass slides and silicon wafers were used as the substrates for AFM and ellipsometry thickness evaluation, respectively. Firstly, the glass slides or silicon wafer were rinsed and pre-treated into the Piranha solution (96% H_2SO_4: 30% H_2O_2 = 3:1 (v:v)) to remove the contaminations and generate the negative charge on the surface of glass slides [*Caution!* Cleaning solution reacts violently with organic materials and should be handled with extreme caution]. The coating procedure is as follows: (1) the glass slide or silicon wafer was dipped into the chitosan dispersion for 5 min (for the first bilayer) and 3 min (for other bilayers); (2) the substrates were rinsed in distilled water for 3 min for removing the excess chitosan; (3) the chitosan coated surfaces were dried by filtered compressed air and dipped into the CNs dispersion for certain time (5 min for the first bilayer and 3 min for other bilayers); (4) the rinsing and drying steps were the same as the one for chitosan. Finally, the different numbers of bilayers were achieved by the recycle of (1)–(4) steps. For the coating on flexible plastic, A-PET films were rinsed with distilled water, methanol, and again distilled water for removing the lipids and other contaminants, dried by filtered air, and submitted to corona treatment (BD-20 high frequency generator, Electro-Technic Products, Inc., Chicago, IL, USA) to increase the surface energy and generate a negative-charge surface. Sequentially, the coating procedure is the same as the one on glass slides and silicon wafer. All of the samples were stored into desiccators at 0% RH ready for following measurements. The pH of chitosan or CNs dispersions is presented next to their name in the figures and text. For example, one bilayer of CS (pH = 4)/CNs (pH = 2) is abbreviated as $(CS_{pH4}/CNs_{pH2})_1$.

2.5. Transparency measurements

The transmittance of the sample was measured at a wavelength of 550 nm, according to the ASTM D 1746-70, by means of a Perkin-Elmer L650 spectro-photometer.

2.6. Atomic force microscopy

An atomic force microscope (AFM, AlphaSNOM, WITec GmbH, Germany) was employed both to systematically study the thickness of the deposited multilayers and to analyze their morphology. For thickness measurements, the LbL coating on glass slides was gently scratched in order to expose part of the glass substrate and thus measure the thickness of the coating. Topography images were acquired with soft tapping mode at low oscillation amplitudes, stabilized by an amplitude-modulation feedback system based on the optical lever deflection method. Standard AFM Si probes have been used.

2.7. Ellipsometry

The thickness of each layer from 0 to 8 bilayers was also determined by a variable angle spectroscopic ellipsometer (VASE® J.A. Woollam Co. Inc., USA) with a wide spectral range capability of 200–1700 nm. In order to provide the system with a standard reference substrate, CS/CNs multilayers were here deposited on a Si wafer. Data were collected at different angles of incidence (60°, 65° and 70°), between 400 and 800 nm. The ellipsometric amplitude ratio, Ψ, and the phase difference, Δ, data were fitted using a Cauchy model for the refractive index of the deposited material, with its given uncertainty based on data reported in the literature (Angles & Dufresne, 2000; Frank et al., 1996; Kasarova, Sultanova, Ivanov, & Nikolov, 2007; Ligler, Lingerfelt, Price, & Schoen, 2001; Sei-ichi, Rumiko, Hideki, & Yoshihito, 2001).

In order to increase the fitting accuracy, the Bruggeman model of the effective medium approximation (EMA) layer was employed (Hoeger, Rojas, Efimenko, Velev, & Kelley, 2011). This approximation allowed for film thickness analysis by incorporating air as an integral part of the ultrathin film. The positive free parameters of the fitting were the thickness of the deposited layers and their percentage P of air-filled voids. The fitting of the experimental data was performed by minimizing the mean-squared-error defined as

$$MSE = \sqrt{\frac{\sum_{i=1}^{N}\left[\left(\frac{\Psi_i^{\mathrm{mod}}-\Psi_i^{\mathrm{exp}}}{\sigma_{\Psi,i}^{\mathrm{exp}}}\right)^2+\left(\frac{\Delta_i^{\mathrm{mod}}-\Delta_i^{\mathrm{exp}}}{\sigma_{\Delta,i}^{\mathrm{exp}}}\right)^2\right]}{2N-M}}$$

where N is the number of measured Ψ and Δ pairs and M is the total number of model fit parameters.

Since the layer thickness and the material refractive index are expected to be correlated in the fitting procedure, the reported thickness values were found within some uncertainty, which reflects the uncertainty in the material refractive index. However, this uncertainty was found to be lower than 1%, with the exception of thicknesses below about 20 nm (with uncertainty of the order of few %).

2.8. Field-emission scanning electron microscopy

SEM observation of the film cross-sections was carried out with a Zeiss Sigma field-emission microscope at 5 kV. The samples subjected to the SEM observation were pre-coated with gold using a Polaron E5100 Coater at 18 mA for 20 s.

2.9. Oxygen barrier properties

Oxygen permeability measurements of coated A-PET films were performed by OX-TRAN® Model 702 (MOCON, USA), complying with ASTM-3985, under the condition of 23 °C and 0% relative humidity (RH). The samples, with a surface of 50 cm^2, were measured at atmospheric pressure. Each sample was conditioned in the chamber for 24 h, and the oxygen transmission rate (OTR) was measured over 1–2 days until it reached a stable value. The PO_2 of the CS/CNs nanocomposite coating in the coated film [i.e., PO_2 (coating)] was calculated using the following equation (Lee, Yam, & Piergiovanni, 2008):

$$\frac{T(\text{coated A-PET})}{PO_2(\text{coated A-PET})} = \frac{T(\text{coating})}{PO_2(\text{coating})} + \frac{T(\text{A-PET})}{PO_2(\text{A-PET})}$$

where T is the thickness of the coating (CS/CNs nanocomposite), A-PET film, or coated A-PET film.

3. Results and discussion

3.1. Layer-by-layer assembly

We first investigated the layer-by-layer self-assembled growth of the CS/CNs nanocomposite. The growth process and the resulting multilayer structure created by polycationic 1 wt% chitosan and polyanionic 1 wt% CNs are sketched in Fig. 1(a) and (b). Hereafter, we will refer to a single CS/CNs assembly as a bilayer. A representative section of the multilayer film, obtained after 30 deposition cycles on an amorphous-polyethylene terephthalate (A-PET) substrate, is shown in Fig. 1(c). Multiple-layer structures are clearly observed, confirming that nano-scale layers were created by the LbL assembly. The thickness of the 30 bilayers CS/CNs coating can be estimated to be ~800 nm on average. We also measured the optical transparency of the same film at 550 nm, obtaining a transmittance of about 70% (representing a reduction of approximately 13% compared to the bare A-PET substrate). Fig. 1(d) demonstrates the high transparency of CS/CNs nanocomposite coating by eye inspection.

3.2. Thickness of CS/CNs nanocomposite coating

After testing many different pH combinations, we found that the CS_{pH4}/CNs_{pH2} is one of the best for both the transparency and oxygen barrier. Under the CS_{pH2}/CNs_{pH6}, on the other side, both of the polymers chains are charged, which results in a lower thickness coating compared with CS_{pH4}/CNs_{pH2}. Here we therefore chose to compare these two combinations that also provide a clear demonstration of the principle behind the different thicknesses observed. In Fig. 2(a) and (b) we show the thickness, obtained by atomic force microscopy (AFM) and ellipsometry, respectively, for films constituted of an increasing number of bilayers and deposited under two different pH conditions (CS_{pH2}/CNs_{pH6}) and (CS_{pH4}/CNs_{pH2}). The two independent thickness measurements give consistent results on each investigated sample. Note that the thickness increase is proportional to the nominal number of deposited bilayers, clearly indicating a stable and replicable growth process. Under the (CS_{pH2}/CNs_{pH6}) deposition conditions, we obtain an average thickness of ~7 nm per bilayer, as shown in Fig. 2(a) and (b) (empty circles), consistent with previous values reported in the literature for a similar pH combination (de Mesquita et al., 2010). Noticeably, the pH conditions of the employed solutions can be suitably controlled as a means to tune the thickness of the individual layers. Indeed, under the (CS_{pH4}/CNs_{pH2}) conditions, we observe a huge change in the thickness of the individual bilayers, which increases from ~7 up to ~26 nm (solid squares).

In order to better understand the role of charges on the growth process, we performed surface charge density measurements by

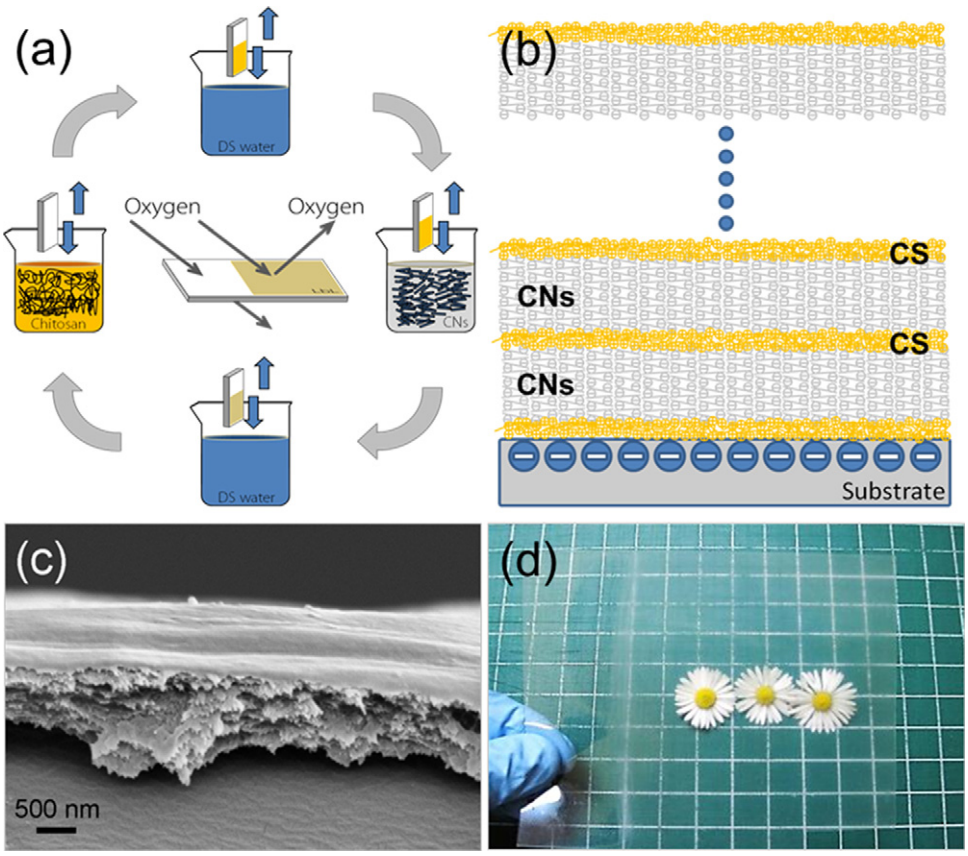

Fig. 1. (a) Illustrations of the LbL self-assembly process and (b) the nanostructure constructed by the alternate adsorption of CS (orange) and CNs (gray) onto a substrate. (c) Scanning electron microscopy image of the multilayer cross section, after cutting it with blade and coating it with a few nm Au layer. The average thickness of the multilayer is about 800 nm. (d) Optical property of coated A-PET. CS, chitosan; CNs, cellulose nanocrystals. (For interpretation of the references to color in this figure legend, the reader is referred to the web version of the article.)

means of conductometric titration at neutral conditions. From such measurements, the amounts of cationic and anionic groups are found to be about 4600 and 220 mmol kg^{-1} for chitosan and CNs, respectively, in good agreement with previous reports (de Mesquita et al., 2010). In other words, the ratio of $-NH_3^+$ (from chitosan) to $-O-SO_3^-$ (from CNs hydrolyzed by H_2SO_4) is about 21. A highly different surface charge density leads to large differences in the chitosan and CNs-layer thickness, as confirmed by Fig. 2(b). Combining the evidence of surface charge density with the thickness values obtained for each individual layer by ellipsometry, we conclude that electrostatic interactions are the main driving force in the LbL assembling of chitosan and CNs and in establishing their thickness. On the other hand, the overcompensation has also to be taken into account as a crucial factor in determining the thickness (Yang et al., 2011), especially under the CS_{pH4}/CNs_{pH2} conditions. In this case, surface charges on the CNs layer are particularly sensitive to local pH, thus the pH of the chitosan solution (pH 4) makes cellulose segments more charged. A similar process occurs for the complementary situation as well, when the chitosan layer is dipped into the CNs solution (pH 2). Eventually, a larger number of charged groups induces overcompensation, thereby significantly increasing the thickness of deposition. As for CS_{pH2}/CNs_{pH6}, if a sample with chitosan top layer is dipped into CNs pH 6 solution, the local pH significantly decreases the charge density of chitosan, leading to much less CNs attracted, thereby a lower film thickness. The same also occurs for the opposite situation (dipping CNs pH 6 into pH 2 chitosan solution). Hence, adjusting the pH of two polyelectrolytes solutions or dispersions can tune both the individual thicknesses and the relative proportion of the two biopolymers, thereby influencing the oxygen permeability of LbL coating (Lee et al., 2008; Svagan et al., 2012; Yang et al., 2011). Control over the pH conditions seems, therefore, an easy way to achieve lower permeability while keeping the number of deposition steps reasonably low.

3.3. Oxygen permeability of CS/CNs nanocomposite coating

The oxygen permeability coefficient of CS/CNs coating only (inset) and the oxygen permeability of the coated A-PET are presented in Fig. 3 for the (CS_{pH4}/CNs_{pH2}) condition, according to the number of bilayers (n) which vary from 0 to 30. Following the thickness increase of LbL coating, the oxygen permeability (PO_2) value of coated A-PET is decreasing dramatically. At 30 bilayers, the PO_2 value of coated A-PET reduces by ~94%, compared to uncoated A-PET, from about 0.2 down to about 0.013 $cm^3\ m^{-2}\ 24\ h^{-1}\ kPa^{-1}$, as a result of the strong electrostatic interaction and hydrogen bonding between chitosan and CNs. In order to have the same oxygen permeability, a bare PET should be about 2.7 mm thick. In the inset of Fig. 3, the reciprocal value of the oxygen permeability coefficient KPO_2 is also reported to highlight the oxygen resistance of the LbL coating only (after subtraction of the PET contribution). It is a remarkable evidence that from 10 to 30 bilayers, i.e. from 260 to 780 nm (double-side coatings of A-PET), this index remains quite stable, hence KPO_2 is approximately constant. We can thus assume that at the testing temperature neither the oxygen diffusion coefficient, nor the oxygen solubility changes in the CS/CNs nanocomposite, which therefore acts as a homogeneous material, independently of the thickness and the number n of bilayers (for $n \geq 10$) (Lee et al., 2008). This is a relevant assessment in order to design LbL self-assembly nanoscale coatings with a specific oxygen permeability and optimized thickness. The most significant

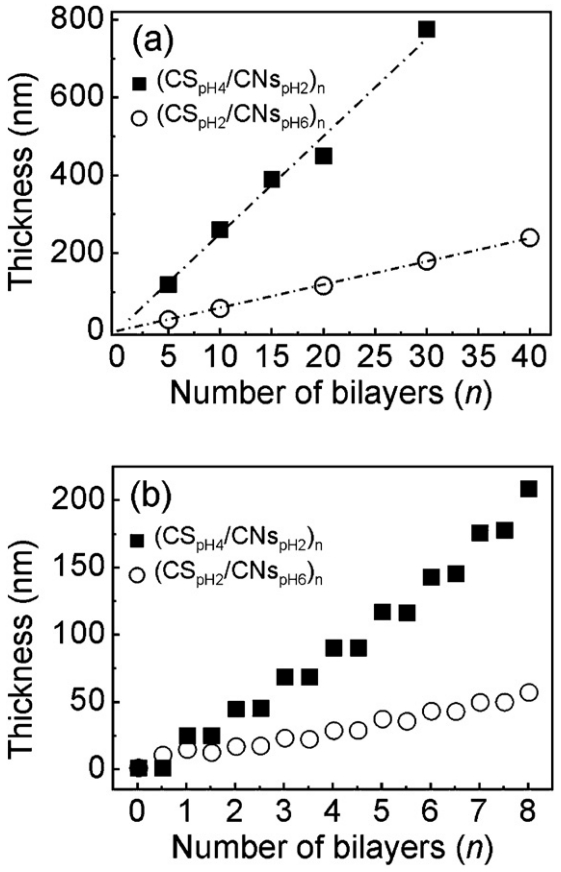

Fig. 2. (a) Thickness, obtained from AFM, as a function of the number of CS/CNs bilayers (n) deposited on a glass substrate at two different combinations of pH values: $(CS_{pH4}/CNs_{pH2})_n$ (■) (dashed line: linear fitting with adjusted $R^2 = 0.996$) and $(CS_{pH2}/CNs_{pH6})_n$ (○) ($R^2 = 0.999$). (b) Thickness, obtained by ellipsometry, as a function of the number of bilayers (n) deposited on silicon wafer for the same conditions as in panel (a). Non integer values of n represent deposition of CS layers, while integer values are related to CNs deposition. CS, chitosan; CNs, cellulose nanocrystals.

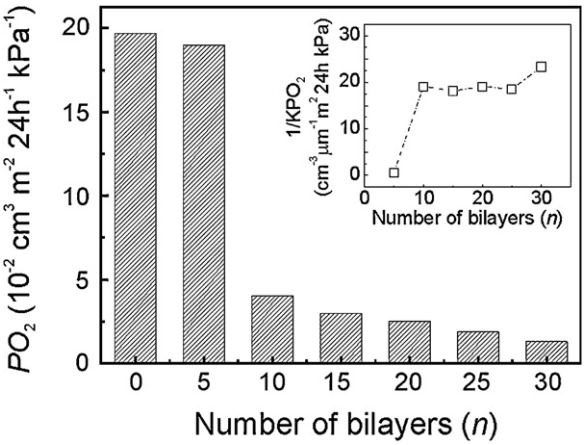

Fig. 3. Oxygen permeability (PO_2, cm^3 m^{-2} 24 h^{-1} kPa^{-1}) for a 180 µm A-PET substrate coated with increasing numbers of $(CS_{pH4}/CNs_{pH2})_n$ bilayers (n = 0, 5, 10, 15, 20, 25, and 30). Inset: reciprocal value of the oxygen permeability coefficient (KPO_2) (cm^{-3} µm^{-1} m^2 24 h kPa) of the bio-nanocomposite coating only. All of the measurements were performed under 'dry condition' (namely, 23 °C and 0% RH). For each number of bilayers, two independent samples were prepared and tested, with typical deviation between the two measurements around 20%. CS, chitosan; CNs, cellulose nanocrystals.

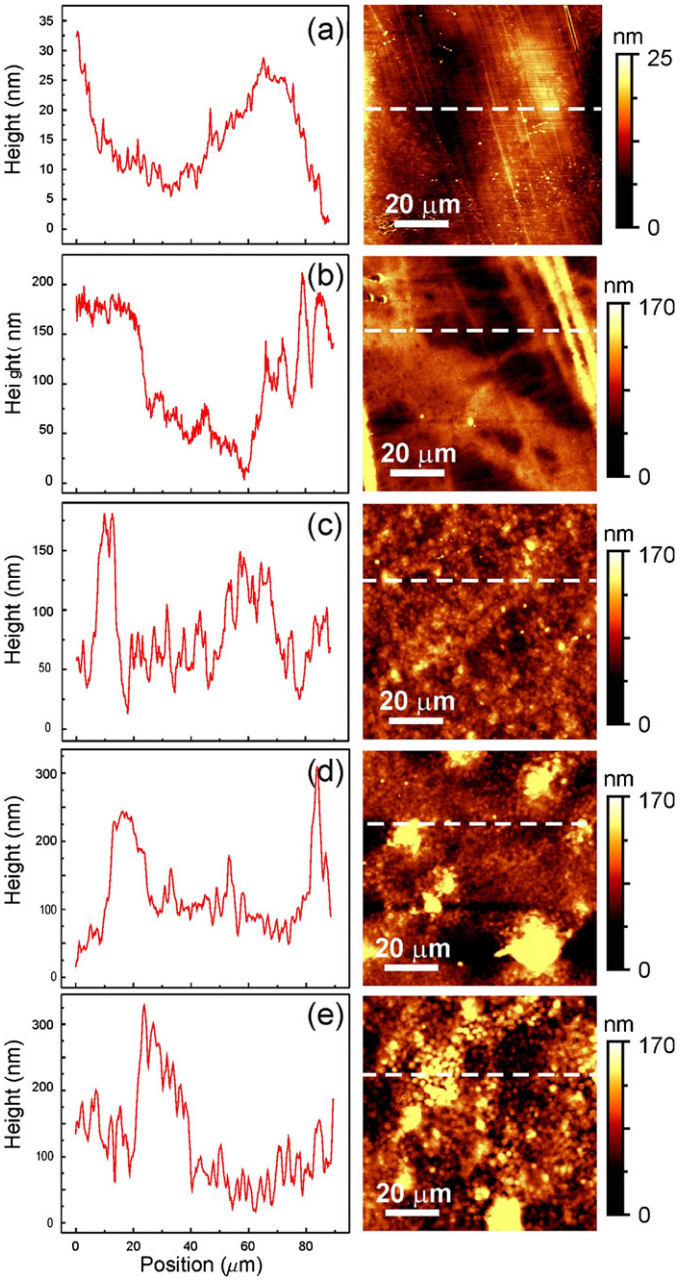

Fig. 4. AFM topography images and section lines of a bare A-PET substrate (a), and the same substrate coated with 5 (b), 10 (c), 20 (d), and 30 (e) CS/CNs bilayers. Note the different height scale bars. CS, chitosan; CNs, cellulose nanocrystals.

decrease of PO_2 value is observed from 5 to 10 bilayers, denoting a likely inhomogeneous structure of the LbL coating for the first 5 bilayers: some pores or extremely thin parts might exist, resulting in easier oxygen penetration. In order to test this hypothesis, we studied the sample topography over (100 × 100) µm^2 areas by AFM. Fig. 4 shows the topography for the bare A-PET substrate (a) and for the coated substrate with 5 (b), 10 (c), 20 (d), and 30 (e) bilayers. Scratches on the bare A-PET surface are likely caused by the friction between films during the handling, but most parts of the PET are smooth. Noticeably, the overall height excursion of the 5 bilayers topography is comparable with the average thickness of the film, denoting a non-uniform coverage of the substrate by the coating, as can also be clearly seen by simple eye inspection of Fig. 4(b). For the 10-bilayer coating, on the contrary, a fully covered surface, with many small CS/CNs aggregates, is apparent from the AFM image, in

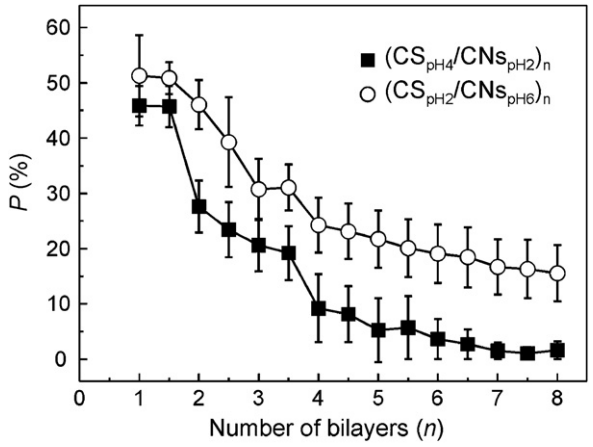

Fig. 5. The air void percentage P as a function of the number of bilayers (n), as obtained from the fitting procedure of the ellipsometry data. CS, chitosan; CNs, cellulose nanocrystals.

qualitative agreement with the results of the oxygen permeability measurements. For the 20- and 30-bilayer samples deposited under the same conditions, the surface topography is qualitatively similar to the one observed for the 10-bilayer film.

The results shown in Fig. 4 are also in agreement with the fitting results of the ellipsometry data. Indeed, in order to increase the fitting accuracy, the Bruggeman model of the effective medium approximation was employed (Hoeger et al., 2011). This allowed for the film thickness analysis (see Fig. 2) by incorporating air as an integral part of the ultrathin film. For the (CS$_{pH4}$/CNs$_{pH2}$) sample, in particular, we found that the percentage of air voids reduces from 30% to 50% for the first two bilayers to less than 6% after the fifth bilayer (see Fig. 5), denoting an increasing filling of the CS/CNs nanocomposite with increasing thickness. This finding is in good agreement with the oxygen permeability results for the (CS$_{pH4}$/CNs$_{pH2}$) sample, which reveal the establishment of good barrier properties only after more than 5 deposited bilayers. Interestingly, similar phenomena have recently been postulated as the reason for the absence of oxygen-barrier properties in a multi-functional LbL coating produced by TEMPO-oxidized cellulose nanofibers and nano-chitin (Qi et al., 2012), where 10 bilayers were deposited with an overall thickness (~100 nm) very similar to our 5 bilayers coating. By our analysis, we are, therefore, able to interpret such occurrence by quantifying the pore density by means of ellipsometry measurements. According to the ellipsometry results, after 8 deposited bilayers the (CS$_{pH2}$/CNs$_{pH6}$) coating was still characterized by more than 15% air voids, which discloses that more LbL cycles are needed to obtain a homogenous nanocoating compared to the (CS$_{pH4}$/CNs$_{pH2}$) conditions.

In this work, the OTR values were measured only under the dry condition and obtained relatively good performance. Since chitosan and CNs are both hydrophilic biopolymers, the oxygen barrier will be certainly reduced under high RH. This limitation is common to the currently used synthetic barrier polymers (polyamide (PA), polyvinyl alcohol (PVOH), ethylene vinyl alcohol (EVOH)) and led to the development of multilayer structures, designed in order to protect moisture sensitive polymers with polyolefin such as low-density polyethylene (LDPE), high-density polyethylene (HDPE), and polypropylene (PP).

4. Conclusions

We demonstrated the use of CS/CNs nanocomposites realized by LbL self-assembly as oxygen barrier under different pH combinations, which has not been systematically reported so far to the best of our knowledge. The oxygen permeability coefficient of CS/CNs nanocomposites is as low as 0.043 $cm^3\,\mu m\,m^{-2}\,24\,h^{-1}\,kPa^{-1}$, close to EVOH co-polymers, under dry conditions (Lee et al., 2008). Although the oxygen barrier property of the CS/CNs bio-nanocomposite is still not as outstanding as that of some LbL coatings including inorganic nanoclays (Svagan et al., 2012; Yang et al., 2011), we consider the absence of any potential risks for human beings and the renewable origin of the carbohydrate polymers as significant added values that justify a deeper investigation and exploitation of the LbL process applied to CS/CNs (Kovacs et al., 2010; Lordan et al., 2011). Moreover, the production processes for chitosan and cellulose nanocrystals are both low-energy consuming, especially compared to microfibrillated cellulose (MFC) produced by mechanical processes (Isogai, Saito, & Fukuzumi, 2011) and the inexpensive use of cotton linters might lead to further promising practical applications. Finally, the chance of finely tuning the oxygen permeability by means of the pH values and the sharp control of the thickness associated with this process also deserve to be underlined. Therefore, based on the advantages outlined above, the LbL CS/CNs nanocomposite represents a promising oxygen barrier component in transparent flexible packaging materials and semi rigid tridimensional objects (bottles, trays, boxes, etc.).

Acknowledgments

We wish to thank Dr. Carmen Roveda and Cesare Pontieri, from Sealed Air (Passirana di Rho, Italy), who carried out most of oxygen permeability measurements, Dr. Gero Bongiorno, from Fondazione Filarete (Milano, Italy), who helped in SEM observations, Dr. Graziano Biagioni, from ILPA (Bazzano, Italy), who provided A-PET sheets, and Alessandro Borghesi for his help during the ellipsometry measurements.

References

Affinito, J. D., Gross, M. E., Coronado, C. A., Graff, G. L., Greenwell, I. N., & Martin, P. M. (1996). A new method for fabricating transparent barrier layers. *Thin Solid Films*, *290–291*, 63–67.

Angles, M. N., & Dufresne, A. (2000). Plasticized starch/tunicin whiskers nanocomposites. 1. Structural analysis. *Macromolecules*, *33*(22), 8344–8353.

Chang, J.-H., An, Y. U., & Sur, G. S. (2003). Poly(lactic acid) nanocomposites with various organoclays. I. Thermomechanical properties, morphology, and gas permeability. *Journal of Polymer Science Part B: Polymer Physics*, *41*(1), 94–103.

Chung, A. J., & Rubner, M. F. (2002). Methods of loading and releasing low molecular weight cationic molecules in weak polyelectrolyte multilayer films. *Langmuir*, *18*(4), 1176–1183.

Cooper, M., Douglas, G., & Perchonok, M. (2011). Developing the NASA food system for long-duration missions. *Journal of Food Science*, *76*(2), R40–R48.

Daiko, Y., Katagiri, K., & Matsuda, A. (2008). Proton conduction in thickness-controlled ultrathin polycation/nafion multilayers prepared via layer-by-layer assembly. *Chemistry of Materials*, *20*(20), 6405–6409.

de Mesquita, J. o. P., Donnici, C. L., & Pereira, F. V. (2010). Biobased nanocomposites from layer-by-layer assembly of cellulose nanowhiskers with chitosan. *Biomacromolecules*, *11*(2), 473–480.

Decher, G. (1997). Fuzzy nanoassemblies: Toward layered polymeric multicomposites. *Science*, *277*(5330), 1232–1237.

Donadi, S., Modesti, M., Lorenzetti, A., & Besco, S. (2011). PET/PA nanocomposite blends with improved gas barrier properties: Effect of processing conditions. *Journal of Applied Polymer Science*, *122*(5), 3290–3297.

Dong, X. M., Kimura, T., Revol, J.-F., & Gray, D. G. (1996). Effects of ionic strength on the isotropic–chiral nematic phase transition of suspensions of cellulose crystallites. *Langmuir*, *12*(8), 2076–2082.

Dvoracek, C. M., Sukhonosova, G., Benedik, M. J., & Grunlan, J. C. (2009). Antimicrobial behavior of polyelectrolyte–surfactant thin film assemblies. *Langmuir*, *25*(17), 10322–10328.

Eichhorn, S., Dufresne, A., Aranguren, M., Marcovich, N., Capadona, J., Rowan, S., et al. (2010). Review: Current international research into cellulose nanofibres and nanocomposites. *Journal of Materials Science*, *45*(1), 1–33.

Etienne, O., Gasnier, C., Taddei, C., Voegel, J.-C., Aunis, D., Schaaf, P., et al. (2005). Antifungal coating by biofunctionalized polyelectrolyte multilayered films. *Biomaterials*, *26*(33), 6704–6712.

Farris, S., Mora, L., Capretti, G., & Piergiovanni, L. (2012). Charge density quantification of polyelectrolyte polysaccharides by conductometric titration: An analytical chemistry experiment. *Journal of Chemical Education*, *89*(1), 121–124.

Frank, C. W., Rao, V., Despotopoulou, M. M., Pease, R. F. W., Hinsberg, W. D., Miller, R. D., et al. (1996). Structure in thin and ultrathin spin-cast polymer films. *Science*, *273*(5277), 912–915.

Fukuzumi, H., Saito, T., Iwata, T., Kumamoto, Y., & Isogai, A. (2008). Transparent and high gas barrier films of cellulose nanofibers prepared by TEMPO-mediated oxidation. *Biomacromolecules*, *10*(1), 162–165.

Ghasemi, H., Carreau, P. J., Kamal, M. R., & Tabatabaei, S. H. (2012). Properties of PET/clay nanocomposite films. *Polymer Engineering and Science*, *52*(2), 420–430.

Hoeger, I., Rojas, O. J., Efimenko, K., Velev, O. D., & Kelley, S. S. (2011). Ultrathin film coatings of aligned cellulose nanocrystals from a convective-shear assembly system and their surface mechanical properties. *Soft Matter*, *7*(5), 1957–1967.

Isogai, A., Saito, T., & Fukuzumi, H. (2011). TEMPO-oxidized cellulose nanofibers. *Nanoscale*, *3*(1), 71–85.

Jang, W.-S., Rawson, I., & Grunlan, J. C. (2008). Layer-by-layer assembly of thin film oxygen barrier. *Thin Solid Films*, *516*(15), 4819–4825.

Kasarova, S. N., Sultanova, N. G., Ivanov, C. D., & Nikolov, I. D. (2007). Analysis of the dispersion of optical plastic materials. *Optical Materials*, *29*(11), 1481–1490.

Kato, Y., Kaminaga, J.-i., Matsuo, R., & Isogai, A. (2005). Oxygen permeability and biodegradability of polyuronic acids prepared from polysaccharides by TEMPO-mediated oxidation. *Journal of Polymers and the Environment*, *13*(3), 261–266.

Kim, B.-S., Park, S. W., & Hammond, P. T. (2008). Hydrogen-bonding layer-by-layer-assembled biodegradable polymeric micelles as drug delivery vehicles from surfaces. *ACS Nano*, *2*(2), 386–392.

Kontturi, E., Johansson, L.-S., Kontturi, K. S., Ahonen, P., Thüne, P. C., & Laine, J. (2007). Cellulose nanocrystal submonolayers by spin coating. *Langmuir*, *23*(19), 9674–9680.

Kovacs, T., Naish, V., O'Connor, B., Blaise, C., Gagné, F., Hall, L., et al. (2010). An ecotoxicological characterization of nanocrystalline cellulose (NCC). *Nanotoxicology*, *4*(3), 255–270.

Lee, D. S., Yam, K. L., & Piergiovanni, L. (2008). *Food packaging science and technology*. Boca Raton, FL, USA: CRC Press.

Leterrier, Y. (2003). Durability of nanosized oxygen-barrier coatings on polymers. *Progress in Materials Science*, *48*(1), 1–55.

Ligler, F. S., Lingerfelt, B. M., Price, R. P., & Schoen, P. E. (2001). Development of uniform chitosan thin-film layers on silicon chips. *Langmuir*, *17*(16), 5082–5084.

Lordan, S., Kennedy, J. E., & Higginbotham, C. L. (2011). Cytotoxic effects induced by unmodified and organically modified nanoclays in the human hepatic HepG2 cell line. *Journal of Applied Toxicology*, *31*(1), 27–35.

Muzzarelli, R. A. A. (2009). Chitins and chitosans for the repair of wounded skin, nerve, cartilage and bone. *Carbohydrate Polymers*, *76*(2), 167–182.

Muzzarelli, R. A. A., Boudrant, J., Meyer, D., Manno, N., DeMarchis, M., & Paoletti, M. G. (2012). Current views on fungal chitin/chitosan, human chitinases, food preservation, glucans, pectins and inulin: A tribute to Henri Braconnot, precursor of the carbohydrate polymers science, on the chitin bicentennial. *Carbohydrate Polymers*, *87*(2), 995–1012.

Nuraje, N., Asmatulu, R., Cohen, R. E., & Rubner, M. F. (2010). Durable antifog films from layer-by-layer molecularly blended hydrophilic polysaccharides. *Langmuir*, *27*(2), 782–791.

Osman, M. A., Rupp, J. E. P., & Suter, U. W. (2005). Gas permeation properties of polyethylene-layered silicate nanocomposites. *Journal of Materials Chemistry*, *15*(12), 1298–1304.

Park, Y. T., Ham, A. Y., & Grunlan, J. C. (2010). High electrical conductivity and transparency in deoxycholate-stabilized carbon nanotube thin films. *Journal of Physical Chemistry C*, *114*(14), 6325–6333.

Priolo, M. A., Gamboa, D., Holder, K. M., & Grunlan, J. C. (2010). Super gas barrier of transparent polymer–clay multilayer ultrathin films. *Nano Letters*, *10*(12), 4970–4974.

Qi, Z.-D., Saito, T., Fan, Y., & Isogai, A. (2012). Multifunctional coating films by layer-by-layer deposition of cellulose and chitin nanofibrils. *Biomacromolecules*, *13*(2), 553–558.

Ravi Kumar, M. N. V. (2000). A review of chitin and chitosan applications. *Reactive and Functional Polymers*, *46*(1), 1–27.

Sanchez-Garcia, M. D., Lopez-Rubio, A., & Lagaron, J. M. (2010). Natural micro and nanobiocomposites with enhanced barrier properties and novel functionalities for food biopackaging applications. *Trends in Food Science and Technology*, *21*(11), 528–536.

Sánchez-Valdes, S., López-Quintanilla, M. L., Ramírez-Vargas, E., Medellín-Rodríguez, F. J., & Gutierrez-Rodriguez, J. M. (2006). Effect of ionomeric compatibilizer on clay dispersion in polyethylene/clay nanocomposites. *Macromolecular Materials and Engineering*, *291*(2), 128–136.

Sei-ichi, M., Rumiko, F., Hideki, I., & Yoshihito, Y. (2001). Change in refractive index of cellulose particle with particle size. *Bulletin of the Faculty of Human Environmental Science, Fukuoka Women's University*, *32*, 65–69.

Svagan, A. J., Åkesson, A., Cárdenas, M., Bulut, S., Knudsen, J. C., Risbo, J., et al. (2012). Transparent films based on PLA and montmorillonite with tunable oxygen barrier properties. *Biomacromolecules*, *13*(2), 397–405.

Yang, Y.-H., Haile, M., Park, Y. T., Malek, F. A., & Grunlan, J. C. (2011). Super gas barrier of all-polymer multilayer thin films. *Macromolecules*, *44*(6), 1450–1459.

Zhai, L., Cebeci, F. Ç., Cohen, R. E., & Rubner, M. F. (2004). Stable superhydrophobic coatings from polyelectrolyte multilayers. *Nano Letters*, *4*(7), 1349–1353.

Zhang, L., & Sun, J. (2010). Layer-by-layer codeposition of polyelectrolyte complexes and free polyelectrolytes for the fabrication of polymeric coatings. *Macromolecules*, *43*(5), 2413–2420.